Macroscopic Quantum Effects in Nanometer-Scale Magnets

David D. Awschalom, David P. DiVincenzo, Joseph F. Smyth

Quantum tunneling, the passage of a microscopic system from one state to another by way of a classically forbidden path, is theoretically possible in the macroscopic world. One can now make direct observations of such macroscopic quantum tunneling in very small magnetic structures. This is possible because of significant advances both in the ability to obtain magnetic systems of almost any desirable size, shape, and composition and in the development of superconducting instrumentation for the detection of extremely weak magnetic signals. As an example, measurements on magnetic horse spleen ferritin proteins with the predictions of quantum tunneling theory are discussed and shown.

The phenomenon of macroscopic quantum tunneling (MQT) exemplifies in its starkest form the clash between the world views provided by classical mechanics and by quantum mechanics. In classical physics, events either definitely happen or definitely do not, and they are independent of the mode by which we observe them. In quantum physics, all events (including classically forbidden ones) happen with some probability, and their likelihood depends on the mode of observation. Tunneling, the passage of a system from one allowed state to another by way of a classically forbidden path, is a familiar example of an event that is describable only in quantum terms. It has been amply demonstrated that quantum processes reign supreme at the length scales of atomic physics and below. However, tunneling even in the macroscopic world (MQT) is theoretically possible (*1*). The claims of quantum theory are all-encompassing: tunneling can occur under any circumstances—a car can indeed pass harmlessly through a mountain rather than be driven over it. Fortunately, such events, which seem impossible on the basis of our everyday experience, are not commonplace for two reasons. First, the mathematical probabilities for these phenomena to occur are very small for large objects; thus, one would only expect to see MQT in "small" macroscopic systems, as in the experiments described below. Second, quantum effects are suppressed if the event is "dissipative" (*1*). Dissipation occurs whenever there is interaction with the outside world by way of a large number of uncontrolled degrees of freedom, such as the "modes" that make up a thermodynamic temperature bath. For this reason, MQT observations require that there be decoupling from the environment to the greatest extent possible, for which ultralow temperatures are often necessary (but not always sufficient).

Despite these difficulties the occurrence of MQT has been thoroughly and quantitatively documented in one system, namely, the Josephson junction [see the review in (*2*); for recent developments, see (*3*)]. In the Josephson junction, two superconductors are separated by a thin insulating barrier; the macroscopic electrical behavior of the junction is completely determined by the difference between the phases of the condensates in the two superconductors. It is found that, despite the fact that a macroscopic number of electrons contributes to the phase degree of freedom, temperature and dissipation can be made low enough that the superconducting phase tunnels: that is, it jumps spontaneously by 2π, even when forbidden to do so by the classical electrical equations. Other quantum effects, such as level quantization, have also been seen.

This review discusses the occurrence of MQT in a very different system: nanometer-scale magnetic systems in which the number of atoms is very large. In this case the macroscopic degree of freedom can be a magnetization direction of a magnetic particle (in so-called "soft" magnets, the case we are most interested in), or the domain-wall position in a magnetic structure (in so-called "hard" magnets). The manifestation of MQT in this case is the transition between two magnetization states, each consisting of ordered lattices of many spins. There is great present interest in the production of small magnetic structures and in understanding and controlling many of their dynamical properties; we have found that such systems are a uniquely suitable area for studying MQT (*4*). Although one normally thinks of technology as being driven by basic science, we will show here how, in recent work, researchers have realized and explored the theoretical concepts of MQT in real systems by exploiting the most recent advances in the technology of low-temperature instrumentation, materials preparation, and magnetic structures.

It was for bulk magnetic crystals that van Vleck and others (*5*) first elucidated the possible dynamical modes of magnets. Above certain critical temperatures, the dynamics are dominated by the thermal agitation of individual spins, resulting in Curie paramagnetism. Below these temperatures, interactions between neighboring spins permit the development of various kinds of ordered magnetic states. Broadly speaking, there are two distinct ordered structures: ferromagnets (FMs), in which the magnetic energy favors alignment of all

Table 1. Overview of the variation in the physical dynamics from classical to quantum at low temperatures in magnetic materials upon reduction of the system's dimension. Classical extends from ~100 μm to ~10 nm; quantum, below ~20 nm. The length scale for the dynamics is dependent on the materials's parameters (for example, saturation magnetization, exchange strength, crystalline anisotropy). Numerical values are representative of common magnetic material. The nature of the dynamics passes gradually from classical to quantum.

Magnetic material	Length scale	Physical dynamics
Bulk crystals	~100 μm	Paramagnetic spin waves
Planar films	~1 μm to 1 nm (thickness)	Nucleation and motion of domain walls
Lithographic patterns	~20 nm	Single domain-wall vortex motion
Scanning tunneling microscopy depositions	~10 nm	Superparamagnetism
Biomagnetic entities	~7 nm	Quantum tunneling
Atomic islands	~1 nm	

D. D. Awschalom and J. F. Smyth are in the Department of Physics, University of California, Santa Barbara, CA 93106. D. P. DiVincenzo is at the IBM Research Division, Thomas J. Watson Research Center, Yorktown Heights, NY 10598.

the spins of the crystal, and antiferromagnets (AFMs), in which the lowest energy state is achieved when neighboring spins point in opposite directions. These ordered states exhibit several different kinds of dynamics: spin waves and the motion of domain walls. Spin waves are small excursions of the atomic magnetic spins around their low-energy state, and excitations of spin waves dominate the low-temperature thermodynamics of magnets. Domain walls are regions in which spins rotate from one direction to another, separating areas of uniform magnetization. The motion of domain walls is of great practical importance; for example, the resistance to such motion determines the strength of a permanent magnet.

Large systems are generally unsuitable for the study of quantum phenomena, mainly because they have many interacting modes of excitation. Therefore, it is very difficult to isolate one of them in order to study its quantum dynamics. Decades of experience in the production and characterization of magnetic structures (*4*) have made it possible to obtain "small" macroscopic magnets of almost any desirable size—7.5 nm in the experiments described below. Table 1 summarizes this progression, which has led to the present opportunity of exploiting magnetic dynamics for the exploration of quantum mechanics. Confinement in a single dimension all the way down to the atomic scale has been possible for some time, through the technique of molecular beam epitaxy as applied to magnetic metals and to magnetic semiconductors. Generally speaking, probing of quantum dynamics becomes possible only when small dimensions can be achieved in all three directions; however, in certain magnetic multilayered structures such as Fe/Sm, tunneling of domain walls in continuous two-dimensional layers of Fe_4Sm has been suggested (*6*). In this and in other experiments, the most common technique has been a study of the "magnetic viscosity," the sluggishness with which the magnetization reverses in response to the change of sign of an external magnetic field. In these experiments it was found that, as the temperature is decreased, the sluggishness increases, but that at very low temperatures the viscosity saturates. From this behavior it has been inferred that quantum tunneling remains available as a mode of relaxation in these systems, but such interpretations are difficult to confirm because of the large degree of uncertainty in the composition of these new materials.

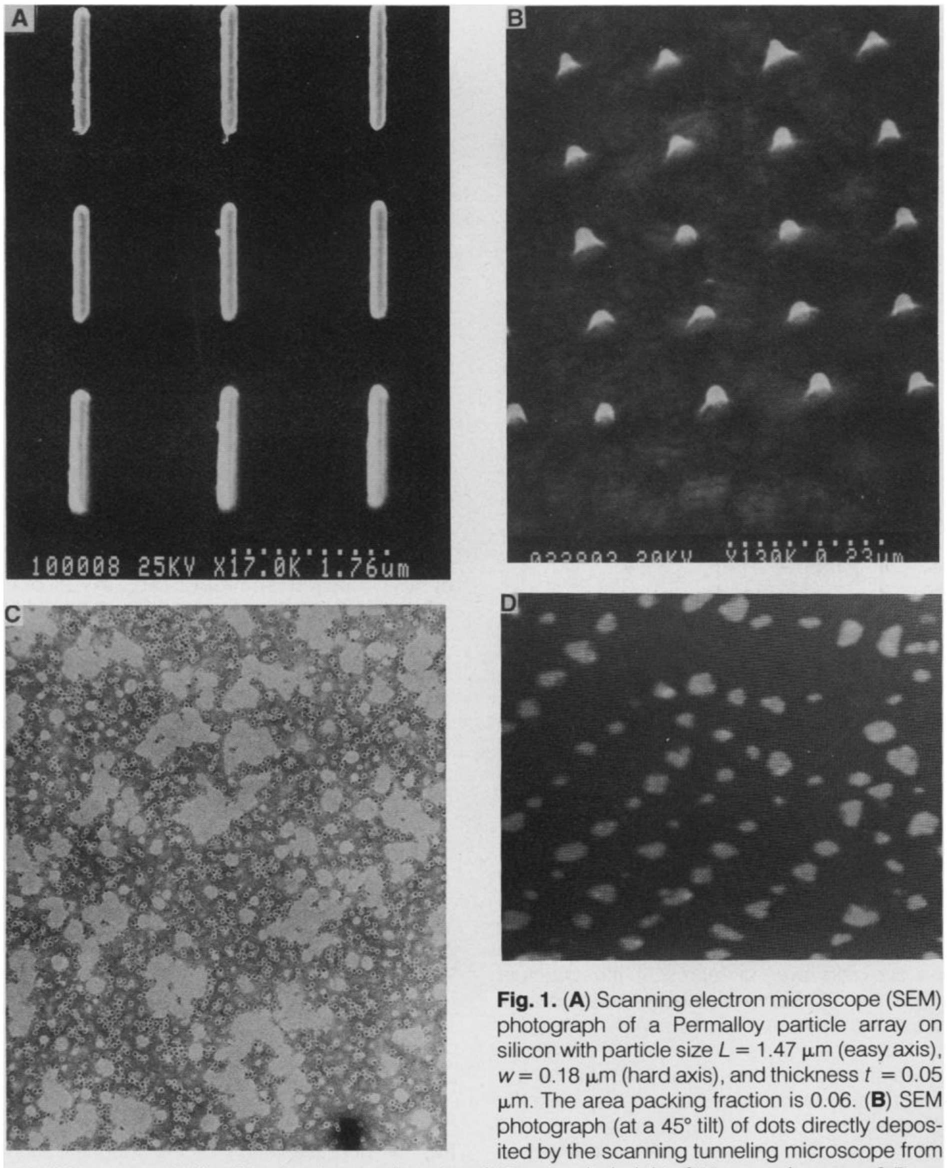

Fig. 1. (**A**) Scanning electron microscope (SEM) photograph of a Permalloy particle array on silicon with particle size L = 1.47 μm (easy axis), w = 0.18 μm (hard axis), and thickness t = 0.05 μm. The area packing fraction is 0.06. (**B**) SEM photograph (at a 45° tilt) of dots directly deposited by the scanning tunneling microscope from $Fe(CO)_5$ on a gold film. The dots have a diameter of 15 nm and a height of 50 nm and are on a 0.5-μm pitch. (**C**) Transmission electron microscope image of horse spleen ferritin proteins with ×80,000 magnification. The inner magnetic core is 7.5 nm in diameter. (**D**) Scanning tunneling microscope image of 0.15 monolayer of cobalt on Au(111). The photograph shows an area of 830 by 710 Å.

Quantum effects in a single "macroscopic" degree of freedom within magnets were actually envisaged over 30 years ago by Swanson (*7*) in the context of future magnetic computer memories. These quantum properties begin to be accessible in structures with dimensions below about 20 nm (*8*). A great challenge is presented by the desire to construct objects of controlled size, shape, crystal structure, and composition on this scale, and a number of methods are available or show promise for accomplishing this task. Sizes down to about 20 nm can be achieved by lithographic techniques; Fig. 1A shows such a structure produced by electron beam lithography in Permalloy, an alloy of Fe (20%) and Ni (80%) (*9*). At these scales it is possible to obtain magnetic particles with simple domain configurations. Such structures should be appropriate for exploring the detailed dynamics of domain walls (*10*), including their nucleation and tunneling. Several experiments using the magnetic viscosity technique have inferred domain wall tunneling in several different systems. Particles of $Tb_{0.5}Ce_{0.5}Fe_2$ as small as 150 Å can be produced by a chemical technique, dispersed within a polymer matrix (*11, 12*). This alloy is believed to be magnetically hard (large magnetic anisotropy, see next section), which means that magnetic domain walls are thin and are likely to be present even in particles of this size. It is not clear in this work how uniform the particle sizes are, or how likely it is that each particle is crossed by just one domain wall. Quantum relaxation has also been inferred in similar magnetic viscosity experiments in multilayer films of Fe/Cu (*6*), Dy/Cu (*6*), Fe/Sm (*13*), and Co/Sm (*14*), in which it is believed that clustering occurs for metallurgical reasons. However, in these experiments it has not been found possible to control or to characterize the particle size distributions.

An alternate technique for making amorphous ferrous particles of somewhat smaller dimensions uses a metallo-organic chemical vapor deposition process that is field-assisted by a scanning tunneling microscope tip in such a way that the deposition only occurs in a sub–10 nm region (*15*); this is shown in Fig. 1B. Another method that has proved successful for obtaining even smaller magnetic structures relies on certain "natural" processes. The particles that are studied in the experiments described herein are produced in horse spleens; these "ferritins," shown in Fig. 1C, serve an iron-buffering and storage function in the animal body, consisting of a protein sheath surrounding a 7.5-nm-diameter crystallite of a hydrated iron oxide closely related to αFe_2O_3 (hematite, a crystalline antiferromagnet) (*16, 17*). Other possible structures that are available for further study include certain fine ferrous particles that occur in soils, magnetic composites (*11*), magnetite particles synthesized by magnetic bacteria, and small clusters of magnetic ions on a nonmagnetic surface produced by various surface deposition techniques (*18*). Recent progress on these latter materials has been reported in the deposition of iron (*19*) or cobalt (*20*) on the Au(111) surface (see Fig. 1D); when done carefully, this process results in ~1-nm particles spaced regularly on the Au(111) surface, separated by similar distances.

Our studies on the dynamics of single-domain magnets at low temperatures focus on the quantum limit of "superparamagnetism." In sufficiently small magnetic particles, especially ones that are magnetically soft (that is, have low anisotropy), the direction of the magnetization points in a single direction across the entire particle. Such a particle is superparamagnetic if this direction fluctuates in time from one preferred orientation to another. In classical physics, at high temperatures, the superparamagnetic fluctuations result from thermal agitation; in quantum physics, at low temperatures, the particle can coherently move from one magnetic orientation to another by tunneling (*7*), and this is the unique example of MQT described here.

Magnetic Theory—Quantum Superparamagnetism

We will consider here the dynamics of both ferromagnetic and antiferromagnetic particles. In an FM, the spins of the constituent atoms are coupled together in such a way that they remain entirely "up" or "down," as seen in Fig. 2; the sum of all these spin vectors is the magnetization **M** of the particle. In the magnets that we will consider (*21*), this magnetization will have two equivalent low-energy directions as indicated in Fig. 2A, separated by an energy barrier that arises from the magnet's anisotropy (crystalline, shape, or surface). Antiferromagnets come in several varieties, but the Néel type is the most common and is well understood. In these, the magnetic coupling is such that neighboring spins prefer to be antialigned (Fig. 2C). The structure can be divided into two aligned sublattices, with magnetization vectors $\mathbf{M}_1$ and $\mathbf{M}_2 \approx -\mathbf{M}_1$. Ferromagnets and antiferromagnets are particularly interesting because their basic dynamical laws are very different from the dynamics of confined particles, yet these systems have dynamics that are different from one another. The action of the magnetization in a potential well is precession rather than oscillation. The classical law of motion for a magnetization **M** is the Bloch equation (*22*):

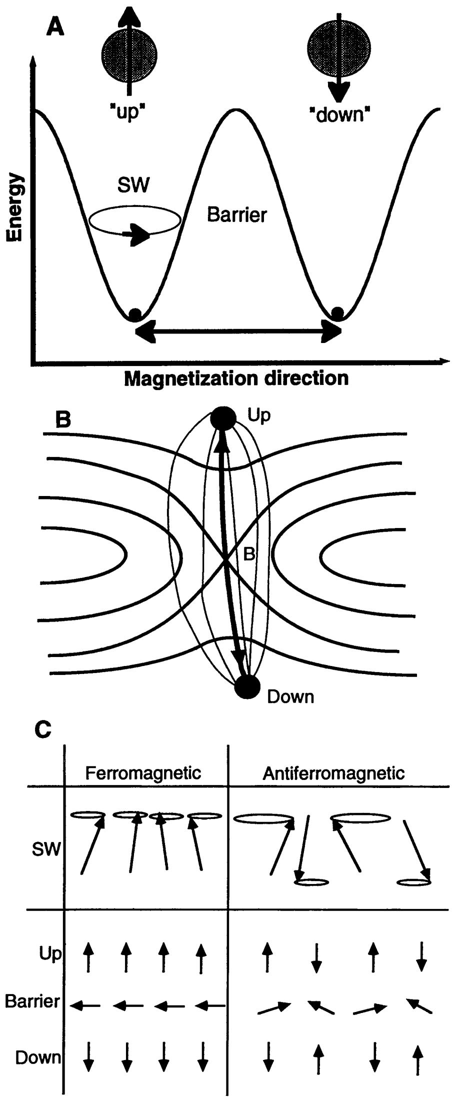

Fig. 2. (**A**) Schematic representation of the magnetic energy *E* versus magnetization direction, indicating two equivalent energy minima "up" and "down" separated by an energy barrier. The circular path labeled SW schematically indicates spin-wave motion. (**B**) Another representation of the energy barrier, with the heavy line indicating the (classical) saddle point path from one minimum to the other. The fine lines suggest the set of Feynman paths that need to be summed over to represent the quantum dynamics. (**C**) Representative arrangements of the atomic spins in the FM and AFM states; SW indicates the circular precession of spins in a wave of magnetization. Below this we show the progression of configurations as the systems progress from the "up" state over the barrier to the "down." The essential difference between the AFM and the FM is that in the "spin wave" and barrier configurations the FM spins remain nearly parallel, whereas in the AFM case their directions become skewed.

$$\frac{d\mathbf{M}}{dt} = -\gamma \mathbf{M} \times \frac{\delta E}{\delta \mathbf{M}} \quad (1)$$

Here γ is the gyromagnetic ratio and E is the magnetic energy (originating, for example, from external fields or anisotropy). In addition, Bloch's equation says that the magnetization precesses in the direction perpendicular to the gradient of the energy, at a rate proportional to the magnitude of this gradient. Figure 3 indicates how such a magnetization vector precesses as a function of time for so called "easy-axis anisotropy," for which there are potential minima for **M** lying in the $\hat{z}$ and $-\hat{z}$ directions. Such motion is a special case of a spin wave.

For a Néel AFM, the classical dynamics are described by two coupled Bloch equations for the two sublattice magnetizations $\mathbf{M}_1$ and $\mathbf{M}_2$ (*22*). In the lowest energy state the two sublattices will be exactly antiparallel (if we assume that the same external field E acts on both sublattices); however, in a dynamical situation ($\dot{\mathbf{M}}_\alpha \neq 0$) one sublattice lags the other slightly. This adds

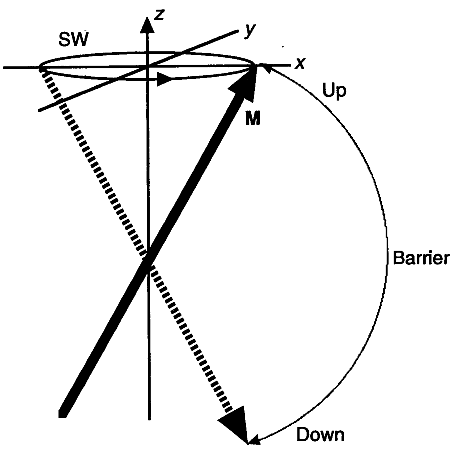

Fig. 3. Representation of the magnetization vector **M**, showing the "up" state, the passage of **M** over the barrier to the "down" state, and the circular precessional motion of the spin wave (SW).

an additional effective term to the energy gradient $\delta E/\delta \mathbf{M}$, which in turn causes a significant speedup of the precession rate, by an amount that depends on the exchange constant J of the AFM (*23*), a constant proportional to the strength of the interaction. The "stiffening" of the AFM relative to the FM is important in the final analysis and is ultimately the reason why the AFM is a better candidate for MQT than the FM (*24*).

The textbook example of this stiffening is found in the properties of the spin waves of the FMs and AFMs (*25*). At low frequency, FM spin waves have very weak restoring forces and do not exhibit typical acoustic dispersion $\omega \sim k$. Instead, $\omega \sim k^2$, where k is the spin-wave wave vector, and $k = 2\pi/\lambda$, where λ is the wavelength of the spin wave. As a consequence, the magnetic interaction energy $J\mathbf{S}_i \cdot \mathbf{S}_{i+1}$ remains low, and this softness is traced to the fact that the individual spins $\mathbf{S}$ in the FM spin wave remain very nearly aligned during their motion, as indicated in the spin-wave (SW) row of Fig. 2C. On the other hand, AFM spin waves exhibit the ordinary $\omega \sim k$ dispersion. This comes from the fact, indicated in the SW column of Fig. 2C, that the neighboring spins remain much less nearly parallel in the AFM spin wave, resulting in a higher energy cost.

A related result, and one that bears very closely on the problem of quantum tunneling, is the behavior of these spin waves in the presence of an anisotropy field (*25*). If the anisotropy is nonzero, then the spin-wave frequency ω no longer goes to zero in the limit of long wavelength; the spin-waves have a finite frequency as $k \rightarrow 0$, the "anisotropy gap." If the scale of the anisotropy energy is K (that is, K is proportional to the energy barrier for the magnetization to pass from the $\hat{z}$ to the $-\hat{z}$ easy axis), then the FM anisotropy gap frequency is $\omega_{\min} \sim K$, whereas that of the AFM spin wave is $\omega_{\min} \sim \sqrt{JK}$. For typical AFMs, the exchange energy density J is of order $J \sim 10^9$ erg/cm^3, while $K \sim 10^5$ erg/cm^3; it is clear that the AFM is much harder than the FM, and this will reflect itself in the quantum tunneling problem.

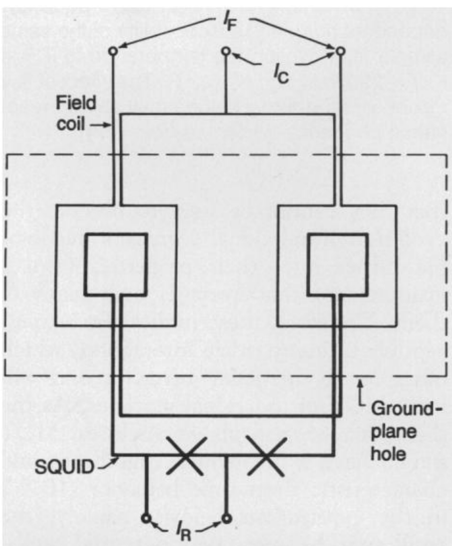

Fig. 4. An integrated dc SQUID susceptometer. The top schematic shows the design configuration of the device built using niobium and lead lithographic processes; I_F, current in the field coil; I_C, current in center-tapped coil; I_R, SQUID bias current. The bottom two photographs display the dc SQUID with planar input transformer, and the square pickup coil structure with coplanar field coils, respectively. The linewidths are 2.0 μm.

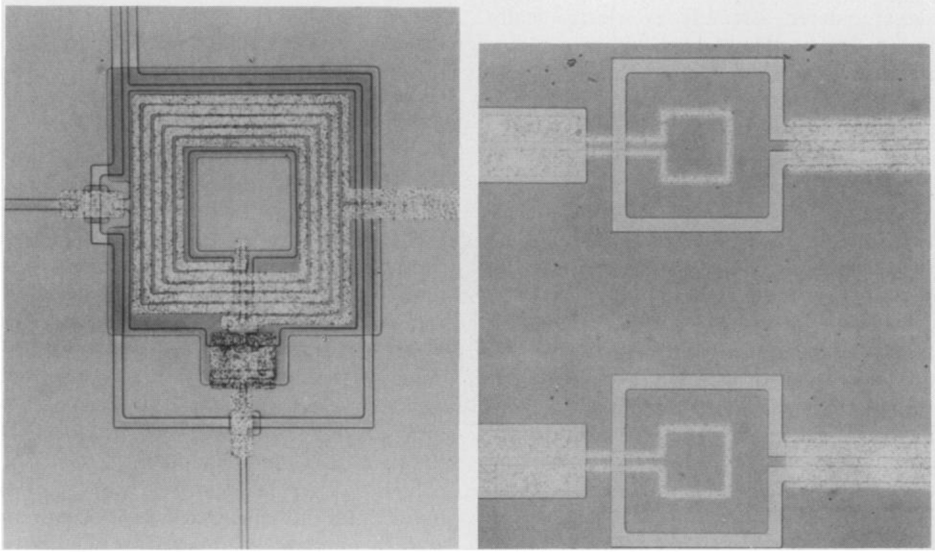

In the absence of any fields and at zero temperature, the passage of magnetization from one anisotropy minimum to another is absolutely forbidden classically on energetic grounds (Fig. 2A). Nevertheless, this behavior has been observed in recent low-temperature experiments, implying the necessity of a quantum theory. One may understand the quantum process by considering all possible routes between an initial and a final state. The dynamics of the magnetization is described as a sum over all possible paths, including those that are classically forbidden like the one that takes $\mathbf{M}$ over its anisotropy barrier, as depicted schematically in Figs. 2 and 3. In this formulation, each path is weighted by the "action" along the path (the action is a measure of the energy in classical mechanics) (*23*).

In microscopic magnetic particles, the action associated with the classically forbidden tunneling paths, and thus their weighting, is small. However, among this set of paths there is one that dominates: it is the "saddle point" path, which passes directly through the valley of the potential-energy surface (depicted schematically in Fig. 2B). Mathematical techniques have been developed to sum up the effects of this path and paths that are related to it by small fluctuations. The result of these calculations is an expression for the rate of tunneling ω between different easy axes. In this "quasi-classical" treatment, the rate ω takes the form (*1, 23, 24*)

$$\omega \approx \omega_0 \exp(-S_I/\hbar) \qquad (2)$$

where S_I, the so-called "instanton action," is obtained from this sum over paths. The prefactor ω_0 is determined by a classical attempt time (that is, the typical spin-wave frequency) and is difficult to determine precisely (*26*).

For this quantum tunneling problem, the difference between FMs and AFMs is determined by the configuration of spins in the saddle point state at point B ("barrier") in the schematic diagram of Fig. 2B and displayed in Fig. 2C. As for the spin waves, the essence of the difference lies in the extent to which the spins remain parallel. In the FM configuration, the spins remain exactly parallel; in the AFM case, the two sublattices are tipped with respect to one another. As a result, the AFM state is less favorable energetically than the FM state, so that the saddle point is passed over more rapidly in the AFM than in the FM state. This makes the instanton action S_I lower for the AFM, and thus the tunneling rate ω is greater for the AFM. As a result, quantum tunneling is easier to observe in AFMs than in FMs.

Ultimately, these calculations yield predictions for this tunneling rate, ω, with the use of the instanton approximation. For the FM it is found that (21)

$$\omega_{FM} \approx \omega_0 \exp(-N_{spin} \sqrt{K_X/K_z}) \quad (3)$$

where N_{spin} is the number of spins in the magnetic particle, and we have introduced anisotropy constants for both the $\hat{z}$ and $\hat{x}$ axes. The AFM result is (24, 27)

$$\omega_{AFM} \approx \omega_0 \exp(-N_{spin} \sqrt{K_z/J}) \quad (4)$$

Because typically $J >> K_{z,x}$, it is indeed true that $\omega_{AFM} >> \omega_{FM}$. The appearance of the number of spins in the exponent means that, for both the FM and AFM cases, the tunneling rate becomes unobservably small if the magnetic particles contain a large number of spins. Thus, we recover the expected result that large systems behave classically and do not exhibit quantum tunneling.

Magnetic Experiments

As an example of the progress that is being made in the study of MQT in magnetic particles, we describe here the results of recent experiments on the low-temperature magnetic dynamics of ferritin particles. The ferritins provide a unique environment in which to explore such physical behavior: they are well studied in the biological community (16, 28) as a result of their importance in mammalian physiology, and one can obtain commercially dense ferritin solutions (interparticle separations of about 20 nm) in which each particle contains about 4500 Fe^{3+} spin-5/2 ions. The particles are basically antiferromagnetic, but, owing to their large surface-to-volume ratio at these reduced length scales, they have a relatively large number of uncompensated surface spins, which permits researchers to probe their dynamics using the coupling of this excess moment to an external magnetic apparatus. These excess spins act as tracers for the AFM particle dynamics. From Mössbauer studies (28) these particles are known to be superparamagnetic below their Néel ordering temperature of $T_N \sim 240$ K. This means that the particle acts as a single domain, and the dynamics are described by a single magnetic vector with a fluctuating direction. Also, from the layered crystal structure of the iron oxide particle, it is likely that the anisotropy has the simple uniaxial form illustrated in Fig. 2. The magnetic interaction between different particles can be continuously controlled by the mixing of the ferritin solution with a solution of apoferritin, a protein whose structure is almost identical to that of ferritin but is nonmagnetic because the iron core is absent. This combination of circumstances presents a favorable situation for probing macroscopic quantum dynamics at low temperatures.

The experiments necessary to observe the magnetic dynamics in ferritin are demanding, because the magnetic signal of a single particle and even of a small droplet of diluted ferritin solution is extremely weak. State-of-the-art superconducting quantum interference devices (SQUIDs) (2) are uniquely suited for making these observations. Recent advances in superconducting VLSI (very large scale integration) technology have led to the development of miniature SQUID gradiometers and susceptometers configured for the detection of small magnetic fields with nearly quantum-limited sensitivity (29). These devices have proven to be valuable tools in the study of both local and global magnetic behavior of low dimensional magnetic structures. We have performed measurements (17) both of the frequency-dependent magnetic susceptibility $\chi(\omega)$ and of the magnetic noise $S(\omega)$ of ferritin proteins using a fully integrated thin-film dc SQUID susceptometer. This miniature planar superconducting circuit is shown in Fig. 4.

In order to reduce the effects of stray magnetic fields, two remotely located series Josephson junctions are connected in a low-inductance fashion to a microfabricated gradiometer detector. This pickup loop structure consists of two square counterwound niobium pickup loops 15.0 μm on a side over a superconducting ground plane, one of which contains a measured sample of magnetic proteins. In addition, a center-tapped field coil, which takes a single square turn around each pickup loop, is used to apply an ac magnetic field (10^{-5} G) for susceptibility measurements as well as to apply static dc fields. The single chip experiment and associated electronics are attached to the mixing chamber of a liquid helium dilution refrigerator and cooled to a temperature of $T \approx 20$ mK. In addition, the susceptometer assembly is electronically and magnetically shielded within a radiofrequency–tight superconducting chamber, and cooled within mu-metal cylinders to achieve a magnetic flux noise of $<10^{-7}\phi_0/\sqrt{Hz}$, where ϕ_0 is the Josephson flux quantum.

As we have mentioned above, many experiments have been performed on the temperature dependence of the magnetic viscosity; these experiments have been used to infer the presence of quantum tunneling at low temperatures (7, 8, 11–14). In this article we concentrate on a new technique, which concentrates on the short time dynamics of magnetic particles. Magnetic viscosity measurements involve measurements on a very long time scale, with relaxations being measured on the scale of seconds. Such measurements are rather indirect, in that they cannot be used to observe the evolution of individual degrees of freedom, but rather infer their properties from a measurement that averages over many of them. Therefore, these studies also are susceptible to interparticle interaction, which often results in glassy behavior and will mask MQT of individual particles. As the theoretical section above discusses, MQT should have a much more significant and characteristic short time behavior (10^{-6} s in the experiments below), namely, the oscillation between two potential wells. When it is possible to see such oscillatory behavior, one should view it as a much more striking and definitive manifestation of quantum behavior than the long-time relaxation.

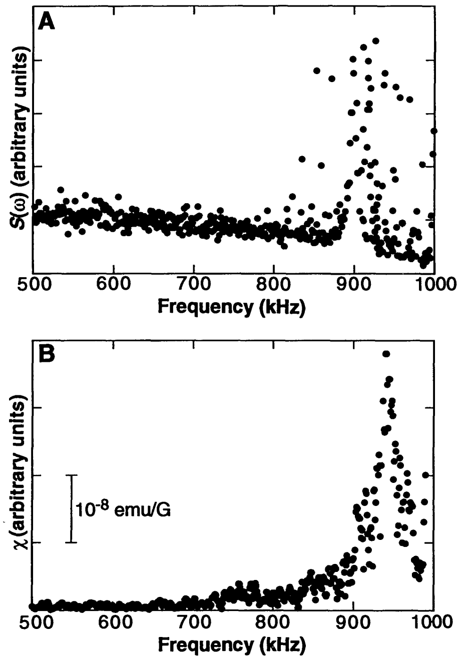

Fig. 5. (**A**) Magnetic noise spectrum of a 1000:1 diluted solution of magnetic proteins; T = 29.7 mK; $B = 10^{-5}$ G. (**B**) Frequency-dependent magnetic susceptibility of the same sample after cycling the temperature to T = 4 K; T = 29.7 mK; $B_{ac} = 10^{-4}$ G. The effect of flux motion is seen through the small shift in resonance frequency. [Adapted from (17)]

The key observation is that, in the more dilute solutions, a well-defined resonance does appear below roughly 200 mK both in $S(\omega)$ and in the imaginary part, $\chi''(\omega)$, of $\chi(\omega)$. This resonance is interpreted as the tunnel splitting between two macroscopic states of the ferritin particles, namely, the Néel vector pointing up and pointing down. The sharpness of the resonance that we observe indicates that dissipative coupling to the environment is weak, one of the important requirements for MQT. The behavior of the resonance as a function of temperature and magnetic field is consistent with theoretical expectations for the occur-

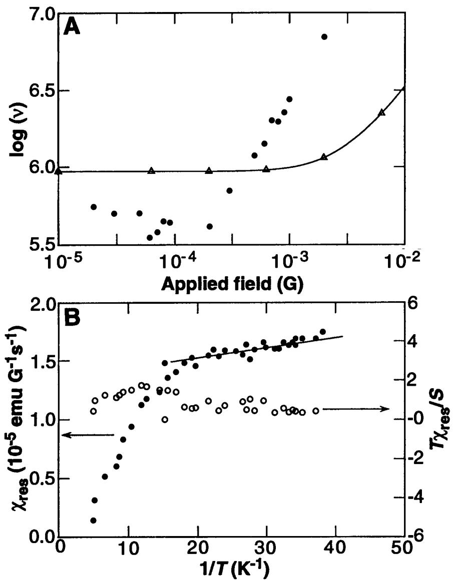

Fig. 6. (**A**) Dependence of the resonance frequency on applied dc magnetic fields; $T = 29.7$ mK. The curve with the Δ symbols is the simple two-level system model of (*1*). (**B**) Temperature dependence of the resonance amplitude in near-zero field ($B = 10^{-5}$ G) showing a linear dependence at low temperature. (There is little shift in frequency.) The quantity $T\chi(\omega_{res})/S(\omega_{res})$ is shown as a check of Eq. 5. [Adapted from (*17*)]

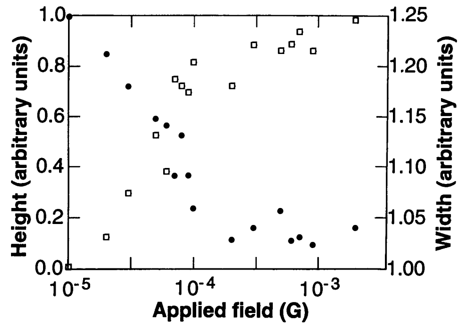

Fig. 7. Behavior of the resonance height (●) and width (□) as a function of applied magnetic field at $T = 29.7$ mK. Both height and width values are normalized to 1.0 at near-zero field conditions ($B < 10^{-5}$ G).

rence of MQT in antiferromagnets.

Figure 5 shows the observed resonance at frequency $\nu_{res} \equiv \omega_{res}/2\pi \sim 940$ kHz in both $S(\omega)$ and $\chi''(\omega)$ for a 1000:1 diluted solution containing ~38,000 magnetic protein particles at 29.7 mK. (Similar results are obtained for 10,000:1 dilution.) Only a single resonance is observed up to the maximum measured frequency of 5 MHz. Finding identical resonant frequencies in these two spectra is an important consistency check, because the two are related by the fluctuation-dissipation theorem (*17*):

$$\chi''(\omega) = (1 - e^{-\hbar\omega/k_B T})S(\omega)/2\hbar$$

$$\simeq \frac{\omega}{2k_B T} S(\omega) \qquad (5)$$

(The second part of Eq. 5 is the high-temperature approximation, which is appropriate for the measurements reported here because $\hbar\omega_{res}/k_B T < 10^{-3}$, where k_B is the Boltzmann constant.) In fact, a slightly higher ω_{res} is obtained from χ'' than from S in Fig. 5; this is attributable to the variation in residual magnetic fields from one run to another or to an imbalance in the on-chip field coils. The resonant frequency is very sensitive to small fields (as is evident from Fig. 6A), even those minute fields trapped within the components of the apparatus, and can only be fixed by cycling the temperature of the superconducting shield after initially cooling the sample. Equation 5 predicts that $T\chi''(\omega_{res})/S(\omega_{res})$ should be independent of temperature.

Figure 6, A and B, shows the behavior of the resonance with the applied magnetic field and temperature. Figure 6A shows that ω_{res} at low temperature is extremely sensitive to minute applied field (by earthly standards); it decreases somewhat up to a field of about 5×10^{-4} G, above which the resonant frequency rises approximately linearly. Figure 7 shows the decrease of intensity and broadening of the resonant peak with applied field. Figure 6B shows the area under the χ'' resonance plotted against $1/T$. At $T^* \approx 200$ mK [T^* is the temperature (roughly 0.2 K in Fig. 6B) below which quantum tunneling through the anisotropy barrier dominates over thermal activation] the resonant peak emerges out of the background, and by about 50 mK the area under the peak increases roughly linearly with $1/T$; ω_{res} is essentially independent of T below 200 mK. Measurements of S and χ'' on an undiluted sample failed to show any resonant structure. We believe that this is a consequence of the appreciable interparticle interactions in the more concentrated material.

Theoretical Interpretation

The above observations can be quantitatively described with the MQT theory (*1*, *7*). If the energy minima of the two macroscopic states are equivalent, which occurs when the external magnetic field is negligibly small and the anisotropy has uniaxial (Ising) character, then the Néel vector performs a simple oscillation between them (*1*), and the magnetization correlation function takes the simple form

$$S(\tau) \equiv$$
$$< M(t)M(t+\tau)> \simeq M_0^2\cos(\omega_{res}\tau) \qquad (6)$$

where ω_{res} is the tunneling rate. Equation 6 predicts resonant behavior for the Fourier transform $S(\omega) \sim \delta(\omega \pm \omega_{res})$, and hence, through the fluctuation-dissipation theorem (Eq. 5), for $\chi''(\omega)$, as seen in the experiment. Here we assume (*24*) that, if the particle has a small number of uncompensated excess spins leading to a magnetic moment M_0, then the dynamics are still determined by the Néel vector **l**, and **M** simply follows **l** as a "slave" degree of freedom. An independent measurement of the excess magnetization of a batch of ferritin particles in the superparamagnetic regime 1 K < T < 240 K below the Néel temperature gives $M_0 = 217\ \mu_B$, where μ_B is the Bohr magneton. This is equivalent to about 43 spin-5/2 Fe^{3+} ions, a small fraction of the $N_{spin} \sim 4500$ spins in the particle, and consistent with the expected number of uncompensated surface spins on such a small particle. Thus, one is justified in assuming that the particle behaves essentially like an AFM.

We can assume that the ferritin particles in the dilute solution tunnel independently of one another (we confirm this with a simple estimate shortly); so, we expect the theory of MQT outlined to apply to the low-temperature observations, at least qualitatively. We now present a set of simple interrelated estimates that support the consistency of the MQT interpretation. We combine Eq. 5 with Eq. 6 for $\hbar\omega \sim \hbar\omega_{res} << k_B T$ to get for the line shape of the lossy part of the magnetic susceptibility:

$$\chi''(\omega) \simeq \frac{\pi N \omega M_0^2}{2k_B T}\delta(\omega - \omega_{res})$$
$$\equiv \chi_{res}\delta(\omega - \omega_{res}) \qquad (7)$$

Here $N \approx 38{,}000$ is the number of ferritin particles estimated to be inside the SQUID pickup. From the slope, $T\chi_{res} \sim 0.9 \times 10^{-7}$ emu·K G^{-1} s^{-1} of Fig. 6B one can solve for M_0 in Eq. 7; taking the observed resonant frequency $\nu_{res} \equiv \omega_{res}/2\pi = 9.4 \times 10^5$ Hz, one finds $M_0 \approx 640\ \mu_B$. This is qualitatively consistent with the results of the high-temperature experiment (though a factor of 3 or 4 higher), in that it supports the idea that the ferritin particles are basically antiferromagnetic, with a small excess spin relative to the total number of iron ions, N_{spin}.

We can use a more drastic but well-justified approximation to the tunneling system to predict some further properties of the quantum tunneling in the presence of an external magnetic field B. This is the two-level system approximation, which was very thoroughly explored by Leggett *et al.* (*1*). In this approach, only the lowest lying states in each of the two wells are taken into account; the effect of all higher lying states on the tunneling dynamics is ignored. This approximation can be justified for sufficiently low temperatures and sufficiently symmetrical wells, but it is difficult to determine a priori how good this approximation will be. We take the optimistic approach and attempt to apply the simplest prediction of the field dependence of the resonant frequency:

$$\nu_{\rm res}(B) \sim [\nu_{\rm res}(0)^2 + (BM_0/h)^2]^{1/2} \quad (8)$$

Taking the standard, high-temperature measurement of M_0, $M_0 = 217\ \mu_B$, as the more accurate, one can see from Fig. 6A that the fit of Eq. 8 correctly matches the overall trend of the data. The two-level system model also predicts that the intensity of the resonant peak will decrease as the external magnetic field decreases the quantum-mechanical hybridization of the two states, and that the signal will broaden because the shift of $\nu_{\rm res}$ will differ for each particle, depending on its orientation with respect to the external field. Figure 7 shows that experimentally both these trends are evident. If taken literally, the two-level system model predicts a somewhat stronger decrease of intensity and a somewhat greater broadening than is observed; any nonideal effects such as protein clustering or alignment will serve to make such predictions uncertain.

We now return to check the assumption that particles can be taken to be noninteracting in the 1000:1 diluted solution, where the typical interparticle distance r_0 is about 200 nm. At these distances the only significant interparticle interaction should be dipolar: that is, each particle produces an effective field $\mathbf{B}_0 \approx \mathbf{M}_0/r^3$ on another particle a distance r away. Assuming that the moments of the various particles point in random directions, we have estimated that (*17*) the typical net field experienced by any given particle is $B_{\rm eff} \approx 2M_0/r_0^3 \approx 5.0 \times 10^{-4}$ G. This is of course a very small field by ordinary terrestrial standards, but it has approximately the maximum value consistent with Eq. 8 and the measured value of the resonant frequency, $\nu_{\rm res} = 9.4 \times 10^5$ Hz, given that $B_{\rm eff}M_0/h \approx 1.5 \times 10^5$ Hz. The same estimate for the undiluted solution, where $r_0 \approx 20$ nm, yields $B_{\rm eff} \sim 0.5$ G, which, according to Eq. 8, would raise $\nu_{\rm res}$ to $\sim 10^9$ Hz, two orders of magnitude higher than the frequencies accessible in these experiments. We believe that this increase in $\nu_{\rm res}$ accounts for the absence of a resonance in the concentrated sample. The interaction energy in the dense solution $B_{\rm eff}M_0$ is equivalent to a temperature of roughly 7 mK. Near this temperature one would anticipate seeing significant interparticle ordering accompanied by a saturation of the low-frequency susceptibility for the concentrated system. In fact, we have seen some effect of local ordering below about 200 mK (*17*). This does not seem unreasonable because we have seen evidence from electron microscope photographs for clustering of the particles, and hence for some stronger local interactions than we assumed in the estimate above.

As a further application of antiferromagnetic quantum tunneling theory (*24*), one can extract estimates of the anisotropy energy K and the transverse susceptibility $\chi_\perp$. As shown in (*24*), $\omega_{\rm res}$ is given by $\omega_{\rm res} \approx \omega_0 \exp(-\sqrt{\chi_\perp K}V/\mu_B)$. Here V is the particle volume and ω_0 is a characteristic microscopic frequency of order 10^{10} s^{-1}. The theory also provides an equation for T^*. This formula is $k_BT^* \approx (\mu_B/2)\sqrt{K/\chi_\perp}$. Solving for $\chi_\perp$ and K in these two equations, we find $K \approx 1.9 \times 10^3$ erg cm^{-3} and $\chi_\perp \approx 5.2 \times 10^{-5}$ emu G^{-1} cm^{-3}. This result for $\chi_\perp$ is very characteristic of this kind of antiferromagnetic materials. The estimate for K is lower than is usually expected by a factor of 10 to 100.

Through their relations to other observable quantities, one can check the self-consistency of these estimates; it is this self-consistency that gives us the greatest confidence in the overall picture of quantum tunneling, more than any one individual estimate. The transverse susceptibility is related to the Néel transition temperature by

$$\chi_\perp \approx \mu_B{}^2 N_{\rm spin}/(k_B T_N V) \quad (9)$$

Using the above estimate for $\chi_\perp$ and taking $N_{\rm spin} = 4500$, one gets $T_N \approx 240$ K, in good agreement with the accepted Néel temperature (*28*). In Mössbauer spectroscopy the blocking temperature T_B is the temperature at which the classical barrier crossing occurs within one Larmor precession time $\omega_L^{-1} \approx 2.5 \times 10^{-9}$ s, and is related to the anisotropy by

$$\omega_L \sim \omega_0 \exp(-KV/2k_BT_B) \quad (10)$$

Using the above estimate for K in this formula, one obtains a blocking temperature T_B of ~ 0.5 K. This is quite low in comparison with reported measurements of T_B of ~ 40 K for horse spleen ferritin, which is a consequence of our rather low value of anisotropy. On the other hand, there are indications that T_B is somewhat variable and is reported as low as 10 K.

Conclusions

To a large degree, this research is motivated by the desire to advance our general understanding of magnetic interactions in matter and, in particular, the influence of quantum mechanics in magnetism. The focus of our work has been in a particular area of magnetic dynamics; however, the investigation of small magnetic structures is only one part of this much larger field. In addition to the many scientific questions that arise in this field, this subject is of practical interest, because much of our information storage capability rests on the ability to measure and control the overturning of spin directions in magnetic storage devices. The physical dynamics occurring in these media fall within the realm of conventional magnetic phenomena; even though track widths are narrower than a human hair, their behavior is typically determined by the classical laws of magnetism. Nevertheless, it is possible that, even in such macroscopic structures, the dynamics of domain wall motion (*10*) or the nucleation of magnetic domains (*30*) at low temperature may be governed by some interesting quantum effects. In addition, this area of physics is important in the fabrication of magneto-optical structures at reduced length scales, where the combination of small magnets and semiconductor technology may lead to a new class of active devices in microelectronics.

This regime of experimental physics addresses fundamental issues in the quantum theory of measurement: how does the act of probing quantum dynamics affect the intrinsic process? In contrast to studies of electronic behavior in semiconductor microstructures or dissipation in superconductors and Josephson junction devices, the physics of magnetism makes it relatively easy to achieve the decoupling from the environment that is necessary for the occurrence of MQT. This is so because local magnetic moments interact very weakly with the most important thermal degrees of freedom in solids such as lattice vibrations (*31*) and conduction electrons; by contrast, observation of macroscopic quantum effects in conduction electrons themselves (in "mesoscopic" electronic devices) has required heroic efforts, because free electrons couple easily with their environment. Magnetic materials offer the promise of making possible the systematic study of the transition from the quantum to the classical regime through variations in temperature, applied fields, material composition, and shape. Other types of magnetic fluctuations are also possible candidates for MQT and have been studied by other workers; these include the motion of magnetic domain walls (*10*), the appearance of small magnetic "bubble" domains (*30*), and even the behavior of individual magnetic ions in a crystal field (*32*).

The making of nearly microscopic magnets is still a challenging problem, and new and unexpected developments are inevitable. Even now, the distinction between "natural" and "artificial" production of these systems is already blurred: if we use a bacterium to make a magnetite particle but do so by biologically engineering the organism and then feeding it a special "diet," is this natural or artificial? What about a tailored biochemical reaction involving specially designed organo-metallic precursors? Currently, the limiting factor for experimentalists is the lack of magnetic materials that are precisely controlled at the atomic scale. Armed with the information available to date, it is extremely important to manufacture micromagnetic structures with a detailed characterization of the particle morphology and of the atomic constituents. Both of these variables play an important role in controlling quantum dynamics in small magnetic structures. Advances in the engineering of micromagnetic materials combined with ongoing theoretical efforts in this area of science make nanometer-scale magnets important tools to help reveal the significance of quantum mechanics in the macroscopic world.

REFERENCES AND NOTES

1. A. J. Leggett *et al.*, *Rev. Mod. Phys.* **59**, 1 (1987); A. O. Caldeira and A. J. Leggett, *Ann. Phys.* **149**, 374 (1983); *ibid.* **153**, 445 (1984).
2. J. Clarke, A. N. Cleland, M. H. Devoret, D. Esteve, J. M. Martinis, *Science* **239**, 992 (1988).
3. S. Han, J. Lapointe, J. E. Lukens, *Phys. Rev. Lett.* **66**, 810 (1991).
4. L. Gunther, *Phys. World* **3**, 28 (1990).
5. J. van Vleck, *Theory of Electric and Magnetic Susceptibilities* (Dover, New York, 1932).
6. L. L. Balcells *et al.*, *J. Magn. Magn. Mater.* **109**, L159 (1992).
7. J. A. Swanson, *IBM J. Res. Dev.* **4**, 305 (1960).
8. P. C. E. Stamp, E. M. Chudnovsky, B. Barbara, *Int. J. Mod. Phys. B* **6**, 1355 (1992).
9. J. F. Smyth *et al.*, *J. Appl. Phys.* **69**, 5262 (1991).
10. P. C. E. Stamp, *Phys. Rev. Lett.* **66**, 2802 (1991).
11. C. Paulsen *et al.*, "Observation of Bloch Wall Tunneling in Small Ferromagnetic Particles," preprint.
12. C. Paulsen *et al.*, *Phys. Lett. A* **161**, 319 (1991).
13. X. X. Zhang *et al.*, *J. Phys. Condens. Matter* **4**, L163 (1992).
14. X. X. Zhang *et al.*, *Phys. Lett. A* **163**, 130 (1992).
15. D. D. Awschalom, M. A. McCord, G. Grinstein, *Phys. Rev. Lett.* **65**, 783 (1990).
16. K. M. Towe and W. P. Bradley, *J. Colloid Interface Sci.* **24**, 384 (1967).
17. D. D. Awschalom *et al.*, *Phys. Rev. Lett.* **68**, 3092 (1992).
18. D. D. Chambliss, R. J. Wilson, S. Chiang, *ibid.* **66**, 1721 (1991).
19. B. Voightlander, G. Meyer, N. M. Amer, *Surf. Sci.* **255**, L529 (1991).
20. ———, *Phys. Rev. B* **44**, 10354 (1991).
21. E. M. Chudnovsky and L. Gunther, *Phys. Rev. Lett.* **60**, 661 (1988).
22. A. H. Morrish, *The Physical Principles of Magnetism* (Krieger, Malabar, FL, 1983).
23. E. Fradkin, *Field Theories in Condensed Matter* (Addison-Wesley, Redwood City, CA, 1991), chap. 5.
24. B. Barbara and E. M. Chudnovsky, *Phys. Lett. A* **145**, 205 (1990).
25. O. Madelung, *Introduction to Solid State Theory* (Springer, New York, 1978).
26. A. Garg and G.-H. Kim. *Phys. Rev. B* **45**, 12921 (1992).
27. I. V. Krive and O. B. Zaslavskii, *J. Phys. Condens. Matter* **2**, 9457 (1990).
28. T. G. St. Pierre, D. H. Jones, D. P. E. Dickson, *J. Magn. Magn. Mater.* **69**, 276 (1987).
29. M. B. Ketchen, M. B. Bhushan, M. B. Kaplan, W. J. Gallagher, *IEEE Trans. Magn.* **27**, 3005 (1991).
30. E. M. Chudnovsky and L. Gunther, *Phys. Rev. B* **37**, 9455 (1988).
31. A. Garg and G.-H. Kim, *ibid.* **43**, 712 (1991).
32. M. Enz and R. Schilling, *J. Phys. C* **19**, 1765 (1986).

33. We are grateful to the IBM Research Division, the Institute for Theoretical Physics at the University of California–Santa Barbara (supported in part by NSF grant PHY89-04035), and the Air Force Office of Scientific Research for their generous support. We thank G. Grinstein and D. Loss who have made important theoretical contributions to this work. We thank M. B. Ketchen and W. J. Gallagher for their helpful design and fabrication of the integrated dc SQUIDs.

The Age and Size of the Universe

Sidney van den Bergh

Modern distance determinations to galaxies were reviewed and placed on a uniform and self-consistent scale. Based on eight separate but not entirely independent techniques, the distance to the Virgo cluster was found to be 15.8 ± 1.1 megaparsec. Twelve different determinations yield a Coma/Virgo distance ratio of 5.52 ± 0.13 and hence a Coma distance of 87 ± 6 megaparsec. With a cosmological redshift of 7210 kilometers per second, this gives a Hubble parameter H_0 (local) of 83 ± 6 kilometers per second per megaparsec. From the velocity-distance relation of rich clusters of galaxies, the ratio of the value of H_0 (global) to the value of H_0 (local) was determined to be 0.92 ± 0.08. In other words, the cluster data do not show a statistically significant difference between the local and global values of the Hubble parameter. If one nevertheless adopts this relation between H_0 (global) and H_0 (local), then the value of H_0 (global) is 76 ± 9 kilometers per second per megaparsec. This observed value differs at the $\sim 3\sigma$ level (where σ is the standard deviation of the distribution) from values in the range $36 \leq H_0 \leq 50$ kilometers per second per megaparsec, which are derived from stellar evolutionary theory in conjunction with standard cosmological models with a density parameter (Ω) that is equal to 1 and a cosmological constant (Λ) that is equal to 0.

The expansion of the universe was discovered with the Mount Wilson 100-inch (2.5-m) telescope by Hubble (*1*) and Hubble and Humason (*2*). During the last decade, it has become clear (*3*) that the velocity-distance relation for galaxies exhibits considerable intrinsic scatter. To determine the present value of the Hubble parameter (H_0) from the relation $V = H_0D$, one must therefore measure the distance (D) of remote galaxies with recession velocities (V) that are at least an order of magnitude larger than the expected deviations from a smooth Hubble flow. However, Hubble noted (*4*, p. 202):

> With increasing distance, our knowledge fades, and fades rapidly. Eventually, we reach the dim boundary—the utmost limits of our telescopes. There, we measure shadows, and we search among ghostly errors of measurement for landmarks that are scarcely more substantial.

In distant galaxies even the brightest objects of standard luminosity are dim and difficult to measure. As a result, the determination of distances to remote galaxies is particularly challenging. This results in considerable uncertainty in the numerical value of the Hubble parameter, which is a measure of the scale size and hence the age of the universe.

Recently, the availability of charge-coupled devices (CCDs) has revolutionized the study of faint stars and galaxies (*5*). The quantum efficiency of CCDs is ~50 times greater than that of the fastest photographic emulsions that had previously been used to study such objects. Furthermore, CCDs are linear panoramic devices with a large dynamic range that are particularly well suited to data reduction by high-speed computers.

In this article, an up-to-date review is given of presently available observational evidence on the extragalactic distance scale. All modern distance determinations have been placed on a uniform and self-consistent scale (*6*, *7*). The recent discoveries of the type Ia supernovae 1991T (which was overluminous) and 1991bg (which was very underluminous) have made it clear that such supernovae cannot be regarded as reliable distance indicators of standard luminosity. In addition, the diameters of supergiant spiral galaxies are not reliable "yardsticks" for measurement of the extragalactic distance scale. The brightest galaxies in some types of rich clusters were found to have a small luminosity dispersion, and these galaxies can therefore be used to place significant constraints on the possible difference between the local and global values of the Hubble parameter.

Here, the plan of attack on the distance scale problem was as follows: first, CCD observations of Cepheids variables, RR Lyrae stars, and other objects of known intrinsic luminosity were used to determine the distances to a small number of key nearby galaxies such as the Magellanic

The author is at the Dominion Astrophysical Observatory, National Research Council of Canada, 5071 West Saanich Road, Victoria, British Columbia, V8X 4M6, Canada.